Breakup of shear-thinning liquids subject to controlled disturbances

A. Dechelette[*1], R. Muddu[2], C. Corvalan[2] and P. E. Sojka[1]
[1]Maurice J. Zucrow Laboratories / School of Mechanical Engineering
[2]Department of Food Science
Purdue University
West Lafayette, IN 47906 USA

Abstract

Shear-thinning solutions were prepared by dissolving different concentrations of Xanthan gum in de-ionized (DI) water or a mixture of DI water/glycerin. The solutions were prepared to have the same zero-shear viscosities (~0.26 Pa.s at 23°C) by adjusting the polymer concentration, from 0% (Newtonian) to 0.10 % wt. (which corresponds to the semi-dilute regime), and the proportion of glycerin in the solvent. 0.5 % wt. of sodium chloride was added to reduce the elastic behavior. Power law indices for these liquids range from 0.44 to 1.0. The liquids were pumped through a piezo-electric nozzle that imposed initial disturbances with dimensionless wavenumbers ranging from 0.2 to 0.8. Jet contours were recorded using high-speed video images and analyzed using camera software. Shear-thinning behavior was found to have a significant effect on drop formation and jet stability. The structure of the jet prior to breakup (beads-on-string) and the consequent formation of satellite drops was dependent on the imposed jet wavenumber for the perturbation amplitude chosen. It was shown that the key rheological parameters governing the satellite formation are the infinite-shear-rate viscosity and the power law index. The zero-shear viscosity had no influence. Finally, comparison to available elastic jet breakup data shows that shear-thinning has an effect opposite to that of elasticity.

Introduction

Breakup of liquid jets has been studied since the work of Savart (1833), Plateau (1873) and Rayleigh (1879), who concentrated on Newtonian liquids. Despite that, and more recent work, it is obvious that there is a lack of knowledge about the breakup of Non-Newtonian jets.

Non-Newtonian fluids behave differently than Newtonian ones because stresses in non-Newtonian fluids have a nonlinear dependence on the rate of strain. Non-Newtonian fluids can also exhibit a time-dependent stress for a constant rate-of-deformation. Non-Newtonian materials are commonly divided into two groups, which are not sharply defined. Fluids that exhibit time-independent behavior are commonly termed "purely viscous". Their rate of shear is solely dependent upon the instantaneous rate of strain. Time-dependent fluids are those for which the shear rate is a function of both the magnitude and duration of the strain rate. The term "viscoelastic" is used because these fluids behave like elastic solids under short time scale deformations, but flow like liquids at large time scales. They also show partial shape recovery upon the removal of a deforming strain.

Non-Newtonian liquids are used in numerous applications, including ink-jet printing, pharmaceutical sprays, food products, and crop spraying. Because of their extended use, it is of interest to clearly understand the mechanisms controlling the breakup and satellite drop formation resulting from breakup of a laminar non-Newtonian jet.

Analytical solutions for the problem of jet breakup are often (if not always) unavailable. Linearization of the governing equations or numerical solutions are then required [1-5]. When dealing with simplified equations, it is necessary to compare with experimental data.

It has been experimentally shown that the introduction of polymers can considerably modify drop formation dynamics. Gordon *et al*. [6] demonstrated that viscoelasticity suppresses formation of satellite drops. It also shortens the breakup length and increases jet instability. In addition, these authors found that the initial disturbance imposed at the nozzle significantly influences drop formation and also determines the presence of satellite drops. The extensive study of Chaudhary and Maxworthy [7] on the effect of wavenumber and perturbation amplitude on the type of breakup (satellite formation, rear merging, front merging, and no satellite formation) showed that an increase in perturbation amplitude generally leads to satellite suppression by front merging. More recently the exhaustive experimental work performed by Mun [8], and by Christanti and Walker [9,10] on jet breakup for different molecu-

[*]Corresponding author

lar weight PEO solutions with the same total viscosities lead to the conclusion that polymer can be used to control the formation of satellite drops. The addition of polymer also decreases the initial perturbation amplitude required to suppress the formation of satellites.

As of now, no experiments have been performed on how low shear-viscosity (or the power law index and the infinite rate viscosity) impacts the breakup of shear-thinning liquids. The aim of this study was to fill this gap by investigating the response of strongly shear-thinning liquids (slightly elastic) to different wavelength perturbations, and then to compare those results to those for a Newtonian liquid with the same shear viscosity as the zero-shear viscosity of the non-Newtonian solutions. The current study also differs from the majority of previous efforts (for inertia dominated jets) because it is the first to employ controlled disturbances for low Reynolds number shear-thinning jets.

Materials and Methods

The fluids are routed through a gear pump (Micropump head GA-X21, Drive 500-4600 rpm) and into a piezoelectric nozzle (University of Erlangen-Nürnberg, Germany, Model LHG-01). The nozzle orifice plate has a 200 μm hole (Melles-Griot). The use of a very thin orifice plate ensures a laminar jet with constant velocity.

Jet breakup is recorded using a high-speed video camera (Phantom V7.3, Vision Research) at either 6688 fps ($\Delta t = 150\ \mu s$) or 10000 fps ($\Delta t = 100\ \mu s$), with 224x600 pixel resolution. Drop shapes are analyzed using the Phantom V7.3 software. Proper illumination was achieved by shining a 500 W halogen lamp into a water container (for IR absorption) that was coupled to an optical diffuser. Room temperature was measured using a thermometer and found to be 23±0.5°.

Shear-thinning liquids were prepared by adding de-ionized (DI) water (three stages of deionization) to Xanthan gum (XG; Keltrol, CP Kelco) powder, and allowing it to incubate for 24 hr at 45°C. NaCl (Mallinckrodt) and glycerin (Mallinckrodt Baker, USP grade) were then added to the water/XG solution and mixed for at least one hour by a magnetic stirrer. Xanthan gum and NaCl quantities were determined using an OHaus balance (Explorer Pro, uncertainty ±0.05mg). The amounts of water and glycerin were determined using a Sartorius balance (uncertainty ±0.05 g). To reduce bacteriological growth, the solutions were stored at 4°C and discarded after two weeks.

Rheological properties were measured on an ARG2 rheometer (TA instruments) with a 40 mm diameter-2° cone for shear rates ranging from 0.005 to 1000 s^{-1}, as well as a 40 mm diameter plate with a 500 μm gap for shear rates larger than 1000 s^{-1}. Shear-thinning fluid parameters were obtained by fitting experimental data to the Carreau model:

$$\frac{\eta - \eta_\infty}{\eta_0 - \eta_\infty} = \left[1 + \left(\alpha\dot{\gamma}\right)^2\right]^{(n-1)/2} \quad (1)$$

where n is the power-law index [-], α is the consistency [s], η_0 is the zero-shear viscosity [Pa.s], and η_∞ is the infinite-shear-rate viscosity [Pa.s].

To make sure that the polymers were not degraded by gear pump head induced high shear deformation, the rheological properties of a 0.1% Xanthan gum solution after 210 min of pumping were compared to the properties measured prior to pumping. Viscosity after pumping was within 5% of viscosity prior to pumping. It was therefore safe to assume that the rheological properties were constant during the experiments.

Fluid densities were determined by weighing a known volume of fluid using a Stratorius balance. Surface tension was determined using a Du-Nuoy tensiometer (Cenco).

A square wave with wavenumber

$$ka = \frac{2\pi a}{\lambda}, \quad (2)$$

and voltage amplitude V=±200V was supplied to the piezo electric crystal inside the atomizer; a is the nozzle radius [m], λ is the disturbance wavelength [m]. Reynolds numbers were determined based on zero-shear viscosity

$$\mathrm{Re}_0 = \frac{\rho U a}{\eta_0}, \quad (3)$$

where U is the velocity at the nozzle exit and ρ is the density.

Results and Discussion

Rheological properties determined using the rotating rheometer are presented in Table 1. Zero-shear viscosities (η_0) range from 221.2 to 269.1 mPa.s. Carreau model parameters are also presented in Table 1. Figure 1 presents the evolution of the solution shear viscosities with an increase in shear rates.

Table 1. Rheological parameters.

Solutions	0.10% wt. XG 0.50% wt. NaCl 99.40% wt. DI water	0.04% wt. XG 0.50% wt. NaCl 59.68% wt. glycerin 39.78% wt. DI water	0.01% wt. XG 0.50% wt. NaCl 87.55% wt. glycerin 11.94% wt. DI water	91.00% wt. glycerin 9.00% wt. DI water
η_0 [mPa.s]	269.1 ± 6.2	237.0 ± 2.6	250.7 ± 2.0	221.2 ± 1.5
η_∞ [mPa.s]	2.2 ± 0.05	9.5 ± 0.1	161.9 ± 1.3	
α [s]	4.7 ± 0.1	8.2 ± 0.09	1.9 ± 0.02	
n [-]	0.44 ± 0.01	0.59 ± 0.006	0.61 ± 0.005	1.00
σ [mN.m]	68.8 ± 0.5	67.4 ± 0.5	69.4 ± 0.5	69.0 ± 0.5
ρ [g/cm^3]	0.98 ± 0.02	1.14 ± 0.02	1.22 ± 0.02	1.20 ± 0.02
Relaxation time [ms]	166	<100	<100	none

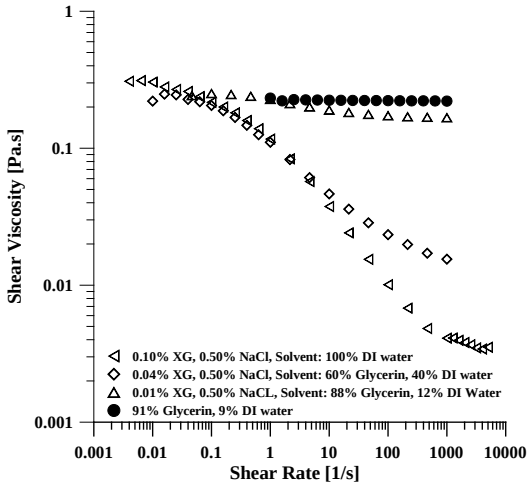

Figure 1. Viscosity of the solutions.

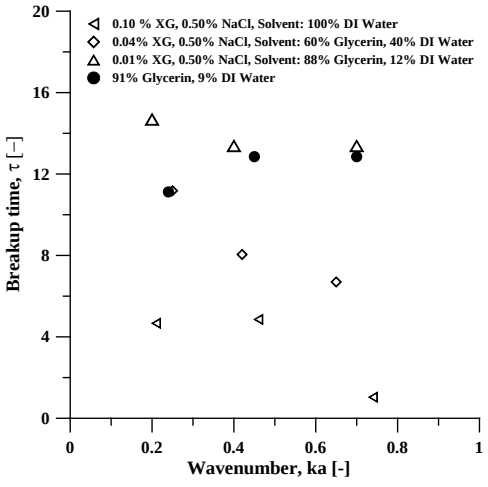

Figure 2. Breakup times.

Uncertainties in the viscosity measurements are within 1% and are not visible if included on Fig. 1. Jet Reynolds numbers ranged from 2.75 to 3.15. They are low enough to ensure non-inertia-dominated behavior, and are the smallest values that can be achieved with the current experimental setup, considering the shear-viscosity of the solutions and the size of the orifice plate.

Results are presented in Figs 2 through 5 for low wavenumber ($0.2<ka<0.4$), medium wavenumber ($0.4<ka<0.6$), and high wavenumber ($0.6<ka<0.8$) disturbances, respectively. The relaxation times for the Non-Newtonian solutions are larger than capillary times ($t_{cap} = a\eta_0 / \sigma \sim 0.5$ ms) so solution elasticity cannot be neglected. However results will be compared to data for both purely elastic jet breakup and to results for filament thinning. This enables us to identify the effect of shear-thinning on breakup dynamics.

Dimensionless breakup times ($\tau = t_{breakup} \big/ t_{cap}$) as presented in Fig 2 are shown to first increase with the addition of a small amount of polymer and then decrease with an increase in polymer (XG) concentration. The first trend can be explained by polymer addition introducing a slight elasticity (inherent to polymeric solutions) which causes the delay in jet breakup. The second trend is the result of the increased shear-thinning behavior with increased polymer concentration. The viscous force magnitude opposing the disturbance growth decreases with concentration and leads to shorter breakup times.

The low wavenumber case breakup data are presented in Fig 3, and show that the four solutions respond differently to high amplitude perturbations. The 0.10%, 0.04% and 0.01% XG solutions exhibit growth of a second harmonic on the filament that in turn leads to the formation of a satellite drop. In the case of the 0.10% XG solution, the satellite drop (Fig. 3.1) does not migrate along the filament, instead forming two secondary filaments that break up to form secondary satellite drops. See Fig 3.1a). In contrast, the satellite drops developing on the 0.04% and 0.01% XG filaments do migrate along the filament and eventually rear-merge with the trailing main drop. This behavior differs from previous experimental studies using either Newtonian or elastic (non shear-thinning) liquids, which all showed that a high amplitude perturbation favors front-merging [7, 10, 11]. The rear-merging observed in this study may be the result of shear-thinning that facilitates drainage of the satellite drop into the trailing main drop. Once rear-merging occurs the filament develops secondary instabilities, as seen in Fig. 3.2c) and Fig. 3.3c). These secondary instabilities have been extensively studied [12] in viscous and viscoelastic threads [13, 14], where it was shown that viscoelastic liquids develop a periodic beads-on-a-string structure. This phenomenon is often termed "filament blistering". Under our experimental conditions, the filament instabilities at the onset of breakup for the two low concentrations are not periodic. This suggests that the drop formation process at the onset of breakup is not elastic-dominated for the 0.04% and 0.01% XG cases, but is instead viscous-dominated so shear-thinning behavior can be considered to dominate elastic effects. Finally the viscous Newtonian jet breaks up without forming satellite drops. Secondary instabilities on the thin filament leads to filament "blistering" similar to that observed for 0.04% and 0.01% XG jets.

A unique satellite drop forms for the 0.10% XG jet under medium wavenumber conditions. As shown in Fig 4, the filament breaks at the leading drop and snaps back into the trailing drop (Fig 4.1b). This also occurs for the 0.04% XG jet, but without satellite formation (Fig 4.2). Finally, both the 0.01% XG and Newtonian jets evolve into a series of main drops connected by a very thin filament. That filament is subject to secondary instabilities, which leads to blistering (Figs 4.3 and 4.4).

At large wavenumbers, the formation of satellites is inhibited for the 0.10% XG jet and the filament snaps back into the trailing drop (see Fig 5.1). This behavior is similar to the 0.04% jet at medium wavenumbers. The 0.04% XG jet at high wavenumbers evolves into main drops connected by very thin filaments (Fig 5.2) which exhibit blistering. Finally both the 0.01% XG and Newtonian jets present interesting features: large liquid elements resulting from drop coalescence (See Figs 5.3 and 5.4) and very thin filaments subject to blistering. When considering the Newtonian jet, the wavenumber of the blobs are observed to be approximately *ka*=0.2. This suggests that there is a second-harmonic of the perturbation developing at the jet interface, and then growing on the low Reynolds number viscous jet. It may be therefore be appropriate to define an infinite viscosity Reynolds number

$$\mathrm{Re}_\infty = \frac{1}{\beta}\mathrm{Re}_0 \quad (4)$$

$$\beta = \frac{\eta_\infty}{\eta_0} \quad (5)$$

This Reynolds number plays a role in the sensitivity of the jet to the perturbation's second harmonic at large wave numbers. The lower $\mathrm{Re}_\infty / \mathrm{Re}_0$, the more sensitive jet behavior is to the second harmonic. For strong shear thinning ($\beta \ll 1$), the shorter wavelength disturbance develops much faster than the long wavelength disturbance and therefore a unique wavelength is observed at the interface. In the case of a weak shear-thinning viscous jet ($\beta \approx 1$), both wavelengths develop at a similar speed and this leads to the structure observed on Figs 5.3a) and 5.4a).

At very large wave numbers (*ka*>0.8), the jets no longer have nearly uniform diameter drops nor filament lengths between adjacent drops. Instead, there is an irregular distribution of drop sizes and filament lengths.

Results obtained for the different solutions suggest that the low shear viscosity is not a key parameter in the jet breakup process, whereas the power-law index and the infinite rate viscosity are key (as shown by the different jet

structures for breakup under the same initial conditions and the four solutions with same low shear viscosities). The lower *n* and β, the more probable the formation of satellite drops. In addition, comparison to available data for viscoelastic jets breaking up points out the importance of shear-thinning in the breakup process. Satellite drops tend to be suppressed for elastic jets. The opposite is observed in this study: the stronger the shear-thinning behaviour, the more probable is satellite formation. Data from Figs 3 through 5 is presented in Fig 6 to illustrate the effect of high-amplitude perturbation on low Re shear-thinning jets as function of the wave number, *ka*. Conclusions from 0.10% XG results are included as well, even though elastic effects are negligible in that case (region I on Fig. 6).

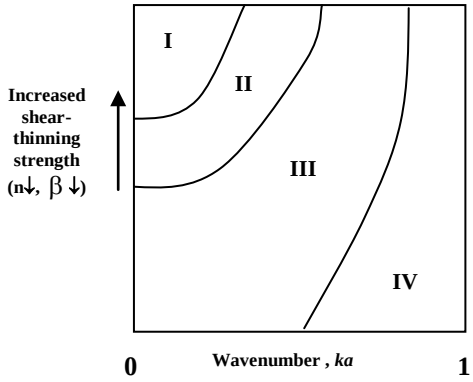

Figure 6. The effect of shear-thinning on jet breakup dynamics for high-amplitude perturbations.

The following regions are included in Fig 5:

I: Satellite drop formation and secondary satellite formation: elastic effect?
II: Satellite formation with rear-merging: filament blistering.
III: No satellite formation: filament blistering.
IV: Unstable jets: coalescence and filament blistering.

Conclusions

Shear-thinning behavior is thought to significantly affect the breakup dynamics of non-Newtonian shear-thinning solutions. However, it was not possible to neglect the influence of elastic effects for the highest Xanthan gum concentration (0.1% XG). Christanti and Walker show that elasticity prevents formation of satellites in the case of purely elastic jets at Re~100. This suggests that shear-thinning effects regulate satellite formation in our case. Finally, it is shown that the zero shear viscosity does not play a role in low Reynolds number jets breakup, but *n* and the infinite rate viscosity do.

In future work, the effect of perturbation amplitude on the same solutions will be studied. Also a strongly shear-thinning solution made from a polymer less elastic than Xanthan gum will be identified and used in order to confirm region I of Fig. 5.

Acknowledgement

This project was supported by National Research Initiative Competitive Grant no. 2008-55112-18797 from the USDA Cooperative State Research, Education, and Extension Service Air Quality Program. The authors would also like to thank Dr. Campanella for his fruitful advice on rheology.

References

1. Goren, S. and Gottlieb, M., *Journal of Fluid Mechanics* 120:245-266 (1982).
2. Brenn, G., Liu, Z. and Durst, F., *International Journal of Multiphase Flow* 26:1621-1644 (2000).
3. Papageorgiou, D., *Physics of Fluids* 7:1529-1544 (1995).
4. Renardy, M/, Journal of Non-Newtonian Fluid Mechanics 59:267-282 (1995).
5. Dravid, V., Loke, P., Corvalan, C. and Sojka, P., *Journal of Fluids Engineering* 130:081504 (2008).
6. Gordon, M., Yerushalmi, J. and Sinnar, R., *Transactions of the Society of Rheology* 17:303-324 (1973)
7. Chaudhary, K.and Maxworthy, T., *Journal of Fluid Mechanics* 96:287-297 (1980).
8. Mun, R., Byars, J. and Boger, D. *Journal of Non-Newtonian Fluid Mechanics* 74:285-297 (1998).

9. Christanti, Y and Walker, L., *Journal of Non-Newtonian Fluid Mechanics* 100:9-26 (2001).
10. Christanti, Y and Walker, L., *Journal of Rheology* 96:733-748 (2002).
11. Vassallo, P. and Ashgriz, N., *Proceedings of the Royal Society Londaon Serie A* 433:269-286 (1991).
12. Brenner, M., Shi, X., Nagel, S,. *Physical Review Letters* 73 (25):3391-3394 (1994).
13. Oliveira, M. and McKinley, G., *Physics of Fluids* 17:071704 (2005)
14. Sattler, R., Wagner, C. and Eggers, J., *Physical Review Letters* 100:164502 (2008).

0.10% XG, 0.50% NaCl, *ka*=0.21 Size: 1.83 mm x 4.90 mm			0.04% XG, 0.5% NaCl, *ka*=0.25 Size: 1.80 mm x 4.82 mm			0.01% XG, 0.50% NaCl, *ka*=0.2 Size: 2.93 mm x 7.86 mm			Newtonian, *ka*=0.24 Size: 2.89 mm x 7.75 mm		
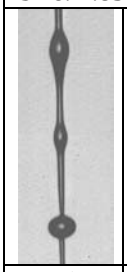	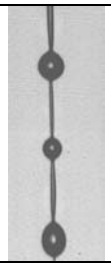	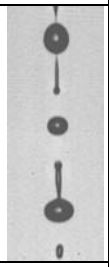			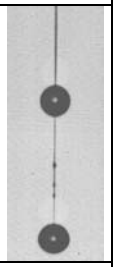			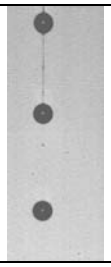			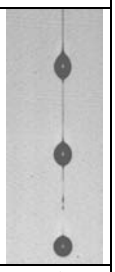
1a) *t*=2.3 ms	1b) *t*=2.83 ms	1c) *t*=3.65 ms	2a) *t*=5.66 ms	2b) *t*=6.76 ms	2c) *t*=7.86 ms	3a) *t*=6.50 ms	3b) *t*=9.67 ms	3c) *t*=10.6 ms	4a) *t*=3.33 ms	4b) *t*=6.81 ms	4c) *t*=7.13 ms

Figure 3. Breakup at low wavenumbers.

0.10% XG, 0.50% NaCl, *ka*=0.46		0.04% XG, 0.50% NaCl, *ka*=0.42		0.01% XG, 0.50% NaCl, *ka*=0.4			Newtonian, *ka*=0.45		
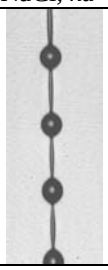			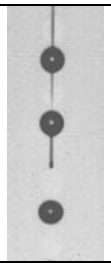			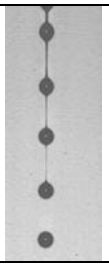			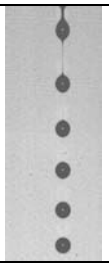
1a) *t*=3.5 ms	1b) *t*=3.8ms	2a) *t*=3.30 ms	2b) *t*=5.66 ms	3a) *t*=3.33 ms	3b) *t*=6.49 ms	3c) *t*=9.67 ms	4a) *t*=3.33 ms	4b) *t*=6.81 ms	4c) *t*=8.24 ms

Figure 4. Breakup at medium wavenumbers (same scale as Fig. 2).

0.10% XG, 0.50% NaCl, *ka*=0.74	0.04% XG, 0.50% NaCl, *ka*=0.65		0.01% XG, 0.50% NaCl, *ka*=0.70	Newtonian, *ka*=0.70
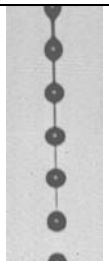	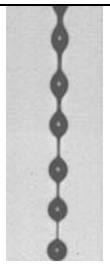	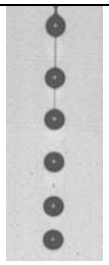		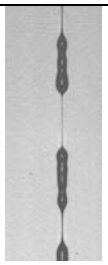
1a) *t*=0.81 ms	2a) *t*=2.8 ms	2b) *t*=4.71 ms	3a) *t*=9.67 ms	4a) *t*=8.24 ms

Figure 5. Breakup at large wavenumbers (same scale as Fig. 2).